applied sciences

MDPI

Article

Numerical Simulation of Surface Subsidence and Fracture Evolution Caused by Pulang Copper Mine Mining

Zhengrong Li [1,2], Kepeng Hou [1], Tong Li [3,4,*], Jingtian Tang [3] and Guangyin Lu [3,4]

[1] School of Land and Resource Engineering, Kunming University of Science and Technology, Kunming 650500, China; lizhengrong-00@163.com (Z.L.); houkepengkm@163.com (K.H.)
[2] Yunnan Diqin Nonferrous Metal Co., Ltd., Shangri-La 674400, China
[3] School of Geosciences and Info-Physics, Central South University, Changsha 410083, China; jtang@csu.edu.cn (J.T.); luguangyin@csu.edu.cn (G.L.)
[4] National Engineering Research Center of High-Speed Railway, Changsha 674400, China
* Correspondence: 225011089@csu.edu.cn

Abstract: Subsidence of the earth's surface induced by mining activities has always been a critical concern in the relevant research fields. This subsidence disrupts the original geological structures and can lead to secondary geological hazards, environmental degradation, and threats to human lives and property. An in-depth investigation of this issue led to us using the three-dimensional finite-difference numerical simulation software FLAC3D 6.0 in this study. The research focuses on the Prang Copper Mine subsidence area in Yunnan Province, China, with a particular emphasis on the comprehensive analysis of the formation mechanisms of a large-scale crack appearing on the south side of the subsidence area. The study also includes a predictive analysis of the future development trends of this crack. The simulation results indicate that the crack formation was a consequence of the combined effects of uneven surface subsidence induced by underground structural interfaces and underground mining activities. As mining activities continued, the non-uniform subsidence of the surface intensified. The northward (Y-axis) displacement difference of characteristic points A and B on both sides of the crack continuously increased, signifying the widening of the crack. Mining activities also influence the displacement in the X-axis direction, potentially posing risks to support structures on either side of existing drainage channels. Therefore, effective control measures are warranted. Furthermore, this study highlights the possibility that new mining activities may further exacerbate subsidence on the south side of the subsidence area. This research provides valuable insights into the complexity of surface subsidence and its associated risks, offering guidance for mining activity planning and safety measures.

Keywords: mining subsidence; numerical simulation; slope; fracture

check for updates

Citation: Li, Z.; Hou, K.; Li, T.; Tang, J.; Lu, G. Numerical Simulation of Surface Subsidence and Fracture Evolution Caused by Pulang Copper Mine Mining. *Appl. Sci.* **2024**, *14*, 2416. https://doi.org/10.3390/app14062416

Academic Editors: Sabrina Bonetto, Pietro Mosca and Chiara Caselle

Received: 7 February 2024
Revised: 4 March 2024
Accepted: 7 March 2024
Published: 13 March 2024

Copyright: © 2024 by the authors. Licensee MDPI, Basel, Switzerland. This article is an open access article distributed under the terms and conditions of the Creative Commons Attribution (CC BY) license (https://creativecommons.org/licenses/by/4.0/).

1. Introduction

Mining resource development brings significant benefits to humanity. However, it inevitably raises a range of safety and environmental issues. Surface subsidence is an essential problem in mining activities, especially in mines using the natural fallout method. Surface subsidence caused by underground mining activities threatens the safety of people and property in the mining area and may lead to secondary geological hazards and damage to the ecological environment. Mining-induced subsidence has been a problem at several mines around the world [1], such as the Ordzhonikidze iron ore mine in Ukraine, where the use of pillar mining in a chamber resulted in the formation of large underground voids, which triggered widespread subsidence and led to a severe mine collapse [2]. The Sechahun Anomaly No.12 in Yazd Province, Iran, also experienced significant subsidence when using the segmented collapse method. In addition, the SLC mining method also led to ground subsidence problems in the western part of the Chengchao iron ore mine [3]. These cases show the severe impact of mining-induced surface subsidence on the mine site and the

surrounding environment. Scholars have employed various methods, including theoretical analysis, physical modeling, field monitoring, and numerical simulation when studying surface subsidence caused by mining activities (Bruneau et al. [4]). In academic research, Hoek et al. [5] utilized limit equilibrium analysis to predict the failure of overlying strata in a mine. In constructing physical models, Ren et al. [6] established a physical model simulating surface and rock mass deformation and monitored surface and surrounding rock displacements with precision. Dai et al. [7] conducted biological model experiments to investigate surface displacement and deformation induced by mining collapses beneath thick loess layers. Physical model experiments can simulate real-world scenarios, provide visual results, and validate numerical models, but they are costly, time-consuming, and subject to scale and parameter limitations. Field monitoring technology offers a direct and effective means of studying surface deformation and rock movement. Field monitoring data can accurately reflect the displacement patterns on the mining surface, guiding mining activities and support design. Xia et al. [8] employed deep borehole extensometers to monitor deformations in the northeastern rock strata of the Jinshandian iron mine, investigating the mechanism of deep rock mass-induced seismic events. Zhao et al. [9] effectively monitored surface deformations and ground fissures induced by mining activities. Based on monitoring results, they discussed the lag and displacement change patterns resulting from mining activity. Other scholars have also conducted research on mining-induced disasters [10–14].

In recent years, with the innovation and advancement of computer technology, the modeling and numerical analysis of complex geological formations have become feasible. As a result, the significance of numerical simulations has progressively gained prominence in addressing complex underground engineering and resource development issues, enhancing engineering safety and efficiency, and optimizing production processes. Standard numerical simulation methods include the Finite Difference Method (FDM, represented by software such as FLAC), the Discrete Element Method (DEM, represented by software like 3DEC), and the Finite Element Analysis (FEA, represented by software such as ABAQUS). Among these, FLAC3D, which employs finite difference principles, demonstrates excellent stability and efficiency and is competitive for numerical simulations of large-scale geological formations. Many scholars have conducted relevant research using FLAC3D. For instance, Yongkui Shi et al. [15] employed FLAC3D to perform numerical simulations of the Jindar coal mine. The research results suggest that numerical simulation methods show a certain degree of reliability compared with the probabilistic integration method results. Nengxiong Xu et al. [16] used FLAC3D to simulate surface subsidence induced by mining activities at the Wutong coal mine, investigating the extent of the subsidence's impact. Parmar H et al. [17] analyzed the influence of surface subsidence caused by mining activities on the surface infrastructure using FLAC3D, providing insights into the extent of the subsidence's effects. Zhao et al. [18] established a three-dimensional finite difference numerical model for the surface topography, ore body, vertical shafts, and major faults of the Jinfeng Gold Mine. They used FLAC3D to assess the stability of vertical shafts and surface deformation caused by the transition from open-pit mining to underground mining. Qian Cheng et al. [19] conducted simulation analyses using FLAC3D to assess surface and surrounding rock damage caused by deep high-dip coal seam mining. Wang et al. [20] employed FLAC3D to simulate mining-induced subsidence and obtained corresponding results. Huang et al. [21] utilized FLAC to predict surface subsidence induced by mining activities and evaluate the effects of different mining methods on dam stability. They also optimized mining schemes. In addition, there are other scholars who have carried out analyses of numerical simulations for a variety of scenarios [22–27].

This study of the impact of new mining operations at the Prang copper mine in Yunnan province was the first of its kind and is relevant to this region. This study utilized FLAC3D software for three-dimensional numerical simulations, exploring the impact of new mining activities at the Prang Copper Mine in Yunnan Province on surface subsidence and crack development. Through the simulation, we aimed to investigate the degree, temporal

evolution, and underlying mechanisms of these impacts, providing a scientific basis for future surface engineering and underground mining activities. This research also aimed to conduct risk assessments to ensure the safety of mining operations.

2. Project Overview

The Prang Copper Mine is in northeastern Shangri-la County, Diqing Tibetan Autonomous Prefecture, northwest Yunnan Province, China. The geographical location of the Prang copper mine is shown in Figure 1. Within the mining area, the geological formations are relatively homogeneous, comprising blocky rock types with a predominance of hard rock and the development of localized fracture zones. This mine uses the natural caving mining method. The Prong Copper Deposit is located within a complex porphyry body, with the ore-containing rock center composed of finely veined impregnated ore and vein-like ore bodies at the periphery. The scale of the ore body is classified as super large, and its morphology is straightforward. The primary elements within the ore body are copper, accompanied by precious metals such as tungsten, cobalt, palladium, and gold. The exposed geological formations in the mining area include the Triassic Tumugou Formation, Prang-type intermediate acid porphyry (mica) rock, and a small number of fourth-series strata. The Tumugou Formation is constructed of volcanic clastic rocks and is divided into three lithological segments based on rock-type combinations. The first lithological segment comprises schistose slate and metamorphic sandstone, interbedded with layers of gray limestone, and schistose slate containing gleaming threads, with a thickness exceeding 400 m. The first layer of the second lithological segment consists of gray to dark gray slate, interbedded with metamorphic sandstone and volcanic angular breccia, with a thickness exceeding 1000 m. The second lithological segment's second layer consists of gray to dark gray slate and acceptable sandy schistose slate, with a thickness exceeding 1000 m. The third lithological segment comprises good sandy schistose slate and crystalline gray limestone with a thickness exceeding 271.4 m. The upper portion of the ore body is covered by Quaternary glacial deposits, with an average thickness of approximately 16.84 m (reaching a maximum of 85.73 m) and a total volume of around 48.47 million cubic meters. While the copper ore body is substantial, it possesses a relatively lower average ore grade and features fault development.

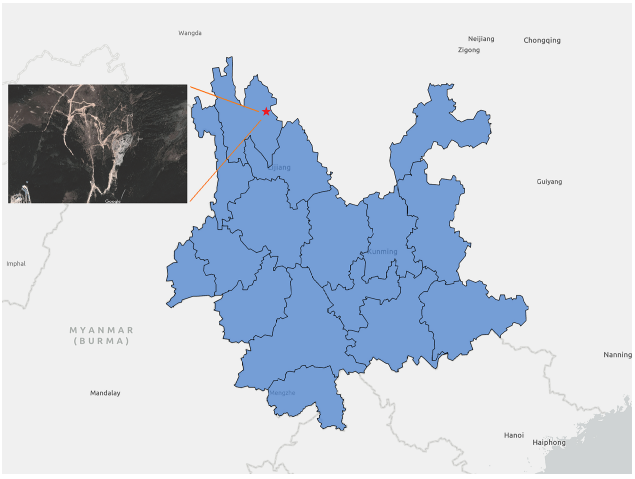

Figure 1. Location of the study area.

Since the commencement of copper mining operations in 2017, ongoing mining activities have led to surface subsidence. During this period, the relevant authorities implemented various measures to address issues in the subsidence area. Presently, the morphology of the study area, as shown in Figure 2, exhibits a circular subsidence crater with a diameter of approximately 400 m. The bottom of the hole is about 3853 m, and a large drainage channel runs along the southern side. Notably, a substantial crack has emerged on

the western slope of the drainage channel, demonstrating a tendency for outward extension and elongation. It is speculated that the formation of this crack is related to the presence of weak planes in the slope and new mining activities in the southern part of the initial mining area.

Figure 2. Aerial view of the study area.

The positional relationship between underground mining and surface subsidence is depicted in Figure 3. Based on this hypothesis, the present study constructed a three-dimensional geological model of the subsidence area and employed three-dimensional numerical simulation methods to analyze and predict the patterns of crack formation and development. This research endeavor will provide valuable insights for future mining and engineering activities.

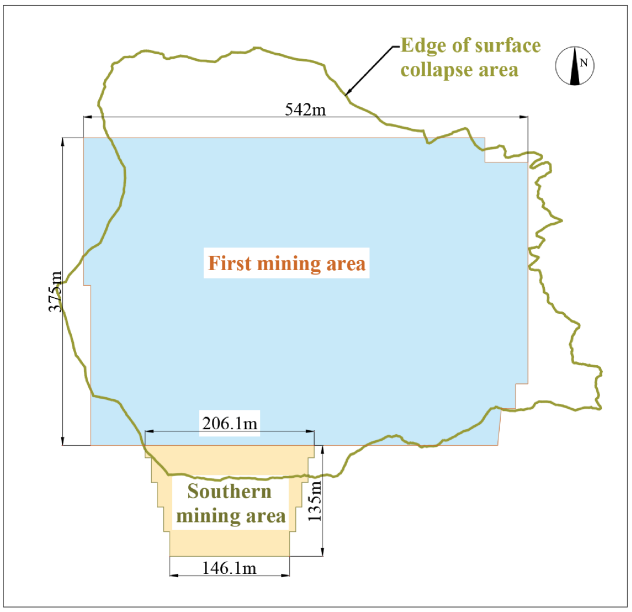

Figure 3. Extent of mining and location of surface collapse.

3. Numerical Simulation Study

3.1. Establishment of Three-Dimensional Geological Model

Based on the latest contour data of the subsidence area and rock strata interfaces, a coupled modeling approach using the Rhinoceros 7.0, Griddle 2.0 , and FLAC3D 6.0 software was employed to establish a three-dimensional geological model of the subsidence area. The model consists of several components, including the overburden layer (glacial deposits), the subsidence area, and the rock strata. The model's spatial coordinates in the Y direction represent true north, with a length of 1045 m in the north–south direction

and 676 m in the east–west direction. The model's horizontal bottom is situated at an elevation of 3690 m. A fully hexahedral grid with grid sizes of 4 m was utilized, comprising 1,725,316 grid cells and 1,345,258 nodes. The 3D model mesh is shown in Figure 4.

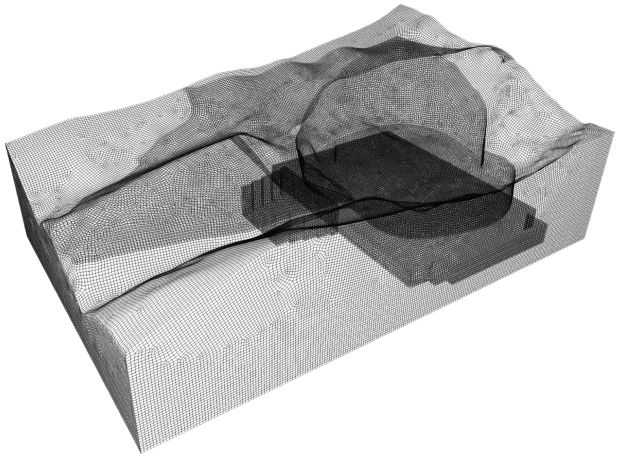

Figure 4. 3D model grid.

The 3D numerical model is shown in Figure 5. It is important to note that a Quaternary glacial deposit cover exists above the ore body, with an average thickness of 16.84 m, reaching a maximum of 85.73 m in certain areas. Since the commencement of mining operations, a significant amount of glacial deposits have entered the subsidence crater as the ore body sank. Additionally, related entities have back-filled some of the Quaternary glacial deposits around the subsidence crater into the mining pit, with some of these glacial deposits infiltrating underground through rock fractures. Consequently, the exact thickness of the glacial deposit layer within the subsidence crater is currently unclear. Based on the analysis of available data, our model establishes the boundary elevation between the upper glacial deposits and the rock strata as 3820 m. Furthermore, in conjunction with information related to underground mining, the model clearly defines the scope of the simulated mining, as illustrated in the cross section of the model in Figure 5b.

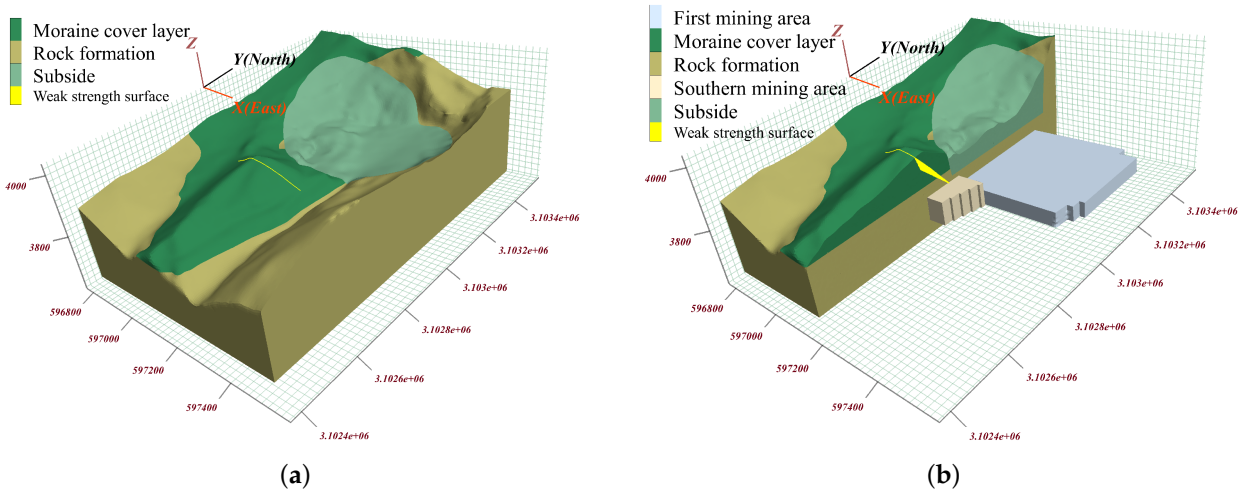

(**a**) (**b**)

Figure 5. (**a**) Three-dimensional geologic model of the study area. (**b**) Three-dimensional model section.

3.2. Selection of Geomechanical Parameters

The rock types within the mining area primarily include quartz diorite, diorite porphyry, and dolomite. Of these, the ore is predominantly found within the quartz diorite, which also constitutes the primary rock type in the subsidence area. Furthermore, the variations in these different rock types' physical and mechanical properties are relatively minor.

To simplify the model, the physical and mechanical parameters of the quartz diorite were used to represent the entire rock stratum. We employed the Mohr–Coulomb elastoplastic model in the numerical simulation calculations. The Mohr–Coulomb strength criterion is a nonlinear material behavior model frequently applied in rock and soil engineering numerical simulations. The following Equation (1) expresses it:

$$f_s = \sigma_1 - \sigma_3 \frac{1+\sin\varphi}{1-\sin\varphi} + 2c\sqrt{\frac{1+\sin\varphi}{1-\sin\varphi}} \quad (1)$$

where σ_1 and σ_3 represent the maximum and minimum principal stresses, and c and φ are the cohesion and internal friction angle.

Due to rock size effects, discontinuities, and environmental complexity, the physical–mechanical parameters obtained from laboratory mechanical tests differed from those of natural rock masses. Therefore, it was necessary to adjust the parameters obtained in the laboratory based on specific criteria. The Hoeke–Brown strength criterion is a commonly used adjustment method [28]. It is derived from rock joints, fractures, structural surfaces, and properties, and combined with extensive practical experience, it can be used to establish the relationship between principal stresses during rock failure; see Equation (2). This criterion is frequently employed for the reduction of rock strength parameters.

$$\sigma_1 = \sigma_3 + \sqrt{m_{\sigma_c}\sigma_3 + s\sigma_c^2} \quad (2)$$

where σ_1 and σ_3 represent the maximum and minimum principal stresses acting on the rock specimen. σ_c denotes the uniaxial compressive strength of the rock mass, while m and s are the material constants of the rock.

The discounted parameters are shown in Table 1 below. In the table, ρ is the density, E is the modulus of elasticity, v is the Poisson's ratio, c is the cohesion, σ is the strength resistance, and φ is the angle of internal friction.

Table 1. Geotechnical physical and mechanical parameters.

	Rock Formation	Moraine Cover Layer	Subside
$\rho/(\mathrm{kg/m^3})$	2760	2100	2100
E / (GPa)	4.5	0.46	0.40
v	0.25	0.11	0.1
$c/(\mathrm{MPa})$	0.88	0.056	0.051
$\sigma/(\mathrm{MPa})$	1.06	0.126	0.110
$\varphi/(^\circ)$	27.8	34.9	32.1

In the model, structural interfaces are represented by thicknessless interface elements within FLAC3D. An elastic constitutive model was employed; the specific structural surface parameters are shown in Table 2 below.

Table 2. Interfacial mechanical parameters.

	Interfacial
Stiffness-shear /(GPa/m)	0.2
Stiffness-normal /(GPa/m)	0.2
$\varphi/(^\circ)$	17

3.3. Boundary Conditions and Numerical Simulation Approach

The model boundaries were constrained using displacement constraints, with normal displacement constraints usual to the sides of the model and displacement constraints in all directions on the bottom surface. In contrast, the model's top was maintained as a free surface. In addition, the model was only subjected to self-gravitational stresses. In the early

modeling stages, the model was intentionally expanded to reduce the constraints' effect on the simulation results in the study area. It should be particularly emphasized that the surface continues to subside during the self-mining process. In the numerical simulation, the model's initial state, i.e., the state of the continuous subsidence of the collapse zone, was represented by applying a constant negative (Z direction) velocity to the top surface of the first mining zone. After several simulations using different Z-direction velocities, the final V-z was taken as 5×10^{-4} m/step. Considering the complexity of the actual strati graphic structure and the uncertainty of the rock state, it was challenging to accurately simulate the natural collapse method of mining using numerical methods. Therefore, this study focused on studying the collapse zone's southern fissure; thus, the model was simplified to a certain extent. The boundary constraints of each orientation of the model are shown in Figure 6 below.

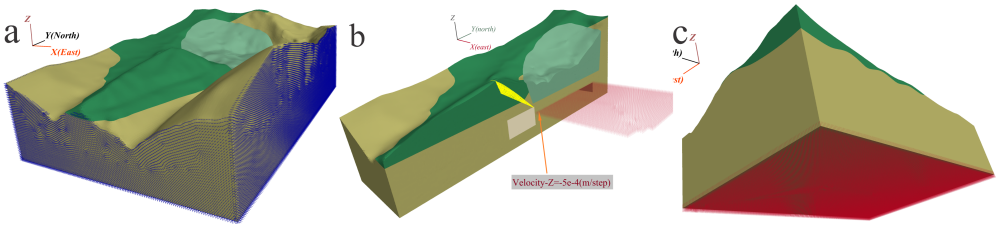

Figure 6. (**a**) Model side constraints. (**b**) Velocity constraints to simulate the original collapse. (**c**) Model bottom constraints.

In its initial state, the model simulated the rock mass excavation in the southern mining area and analyzed the process of mining-induced collapse. It investigated the slope's crack formation and development patterns under new mining conditions. It conducted a comparative analysis of the impact of mining on the existing subsidence crater.

3.4. Analysis of Numerical Simulation Results

Initially, the model involved excavating the southern mining area and then underwent a simulation of 4000 steps under self-weight stress. As shown in Figure 7, this simulation generated a series of displacement contour maps, each representing the model's displacement status at 1000, 2000, 3000, and 4000 steps.

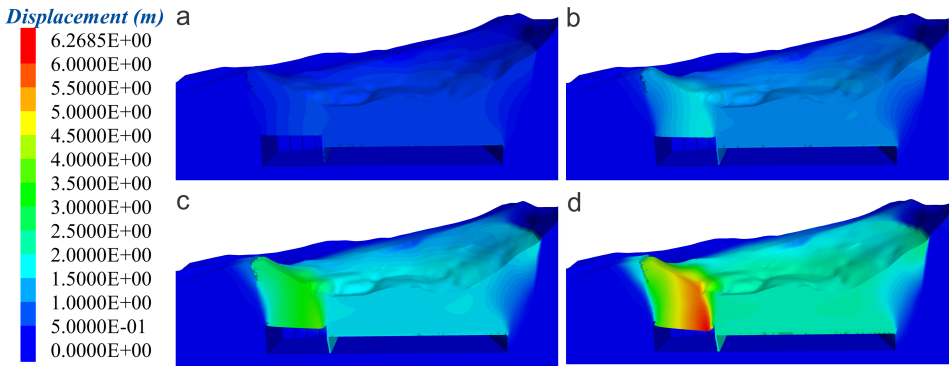

Figure 7. Displacement cloud for each stage of numerical simulation. (**a**) 1000 steps. (**b**) 2000 steps. (**c**) 3000 steps. (**d**) 4000 step.

Comparative analysis of the displacement contour maps at 1000 and 2000 steps revealed that, due to a lack of support and the influence of pre-existing subsidence, areas close to the subsidence zone experienced displacement earlier than other areas. Moreover, the magnitude of displacement in these regions was also the most significant.

The displacement cloud in each direction is shown in Figure 8.

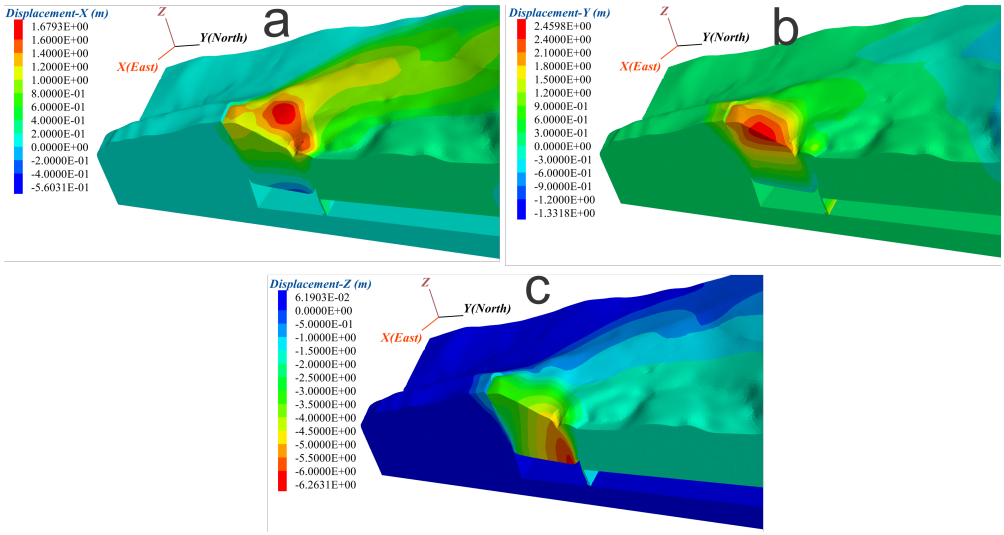

Figure 8. Displacement cloud at 4000 steps in each direction. (**a**) X. (**b**) Y. (**c**) Z.

Observing the displacement cloud maps at different stages, it is evident that, as mining-induced collapse progressed, surface subsidence gradually extended to the south. This non-uniform subsidence may lead to the formation of tension cracks consistent with the actual conditions in the study area. As shown in Figure 9, multiple cracks already existed on-site, further corroborating the results of the numerical simulations.

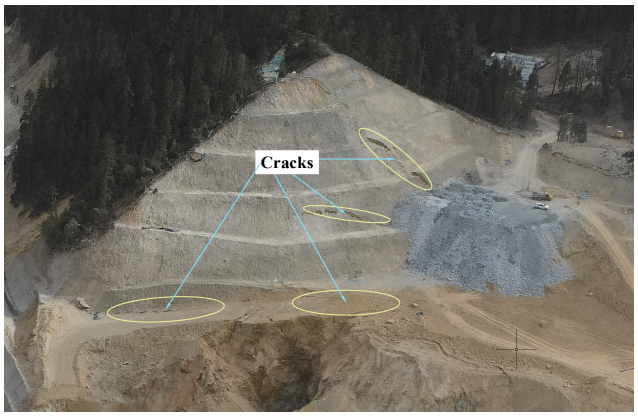

Figure 9. Diagram of fine tension cracks on the south-side slope.

As mining-induced subsidence developed, its effects gradually extended into the internal structural weak planes within the rock and soil mass. These weak planes, characterized by their lower strength, impeded the effective transmission of stress, leading to disparities in displacement in various directions. This process led to the evolution of weak surfaces in the geotechnical body into fissures, which, in turn, evolved into larger cracks. Based on the displacements and displacement differentials recorded at points A and B on both sides of the model interface, as depicted in Figure 10, it is evident that, with the progression of subsidence, both points A and B exhibited a certain degree of displacement. However, these two points had significant displacement disparities within the rock and soil mass. In particular, in the Y (north) direction, the displacement differential gradually increased, leading to the widening of cracks. In the Z direction, the increasing displacement differential resulted in an observable vertical offset between the two sides of the cracks, manifesting as distinct uneven subsidence. The results from the numerical simulation after 4000 steps revealed that the width of the cracks at the top reached 0.6 m, with a vertical offset of 1.8 m. Furthermore, from Figures 8 and 10, it can be observed that mining-induced surface subsidence led to displacement in the X direction on the south slope, potentially impacting the stability of the existing support structures in the drainage channel.

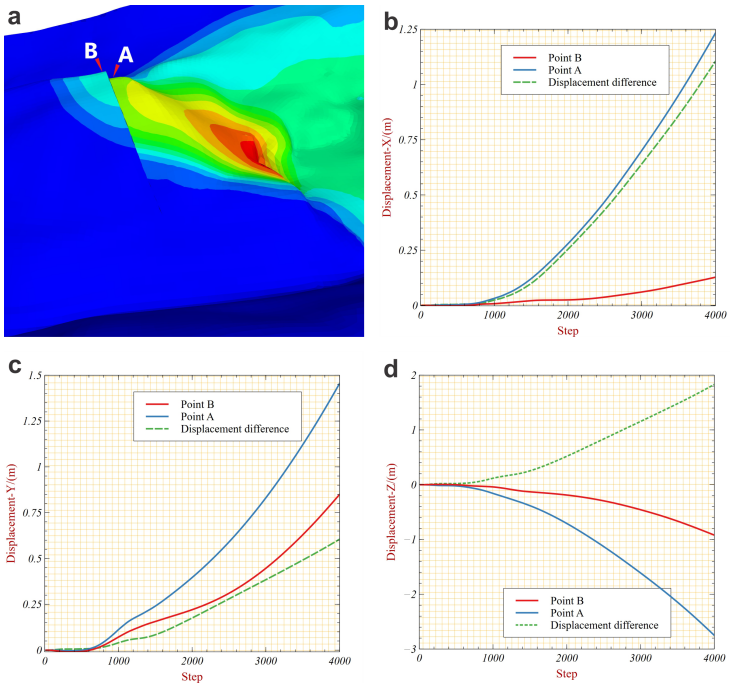

Figure 10. Numerical simulation of monitoring sites. (**a**) Point A and B maps. (**b**) X direction. (**c**) Y direction. (**d**) Z direction.

Furthermore, a comparison was made between the displacement contour maps for the simulation of mining in the southern area and the displacement contour maps for the model only considering the initial state (as shown in Figure 6), both computed after 4000 steps. Figure 11 presents these displacement contour maps for both scenarios. The research results indicate that the displacement was significantly increased in the upper specific region within the southwest part of the subsidence crater, corresponding to the southern mining area. In contrast, the impact in other areas was relatively minor. This observation may be related to the simplified setup of the initial model. However, in practical production, it is still crucial to closely monitor the potential effects of new mining activities on the existing subsidence area.

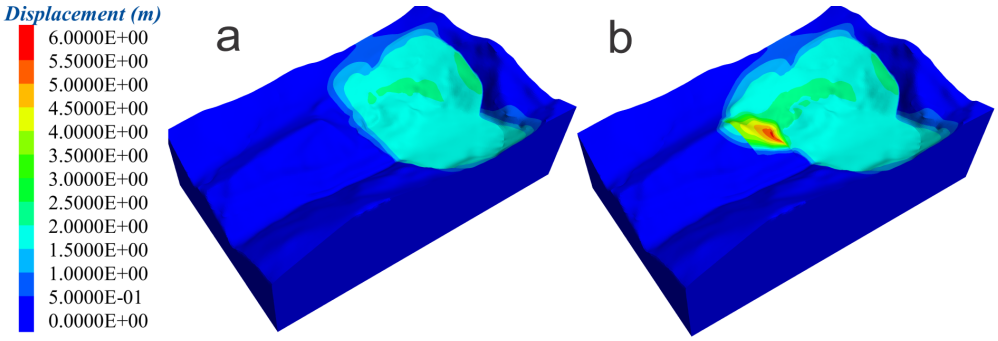

Figure 11. Contrasting displacement cloud. (**b**) No-excavation displacement maps. (**a**) Displacement cloud map of the southern mining area of the excavation.

3.5. Comparison and Analysis of Numerical Simulation Results and Actual Monitoring Data

A GNSS monitoring station on the south slope was installed for displacement monitoring, with its precise location illustrated in Figure 12. Specific monitoring equipment was placed at the center of the slope, as there was less interference from the site. We compared the recorded displacement data from this monitoring device and the simulated displacement data from the equivalent site within the FLAC3D model. The comparison results are as follows.

Figure 12. Location map of on-site monitoring equipment.

The displacement data from a continuous 1000 h of on-site monitoring were compared with the numerical simulation results, as shown in Figure 13. It was observed that the displacement curves of the monitoring data and numerical simulation results exhibited similar trends. In the initial stage, both sets of displacement curves displayed minimal displacement, indicating a certain degree of lag in the surface subsidence induced by mining activities. This observation was further corroborated by the numerical simulation results at different stages, as illustrated in Figure 7. Both monitoring data and numerical simulation results demonstrated significant displacements in the Y and Z directions, with relatively more minor displacements in the X direction.

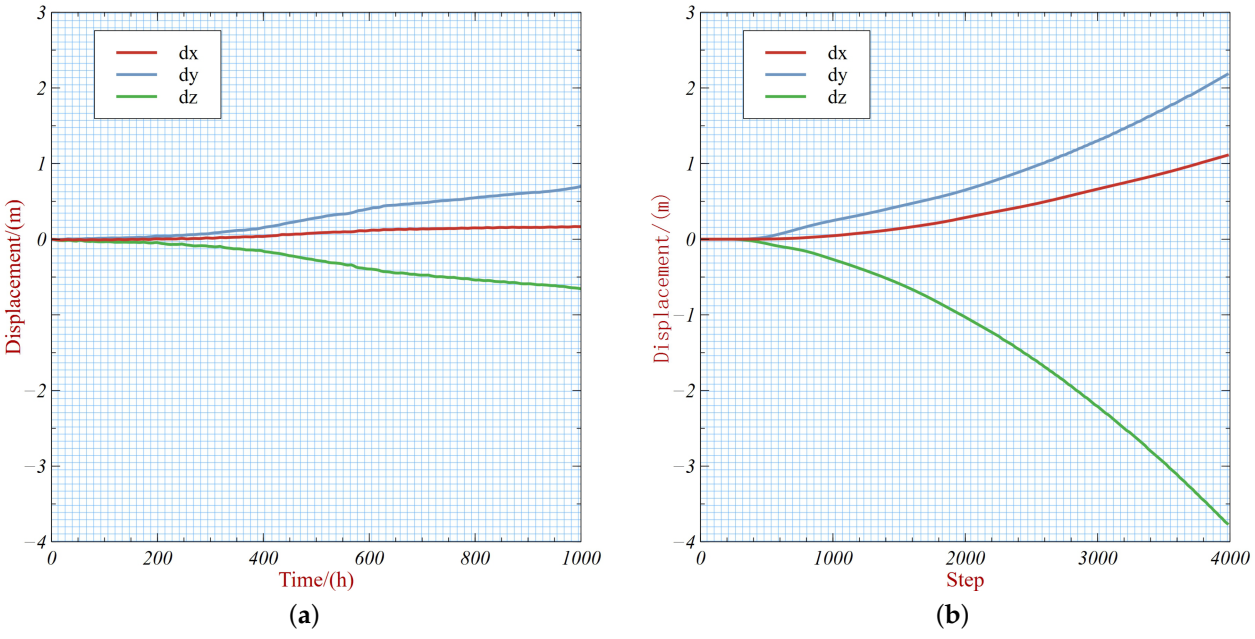

Figure 13. (**a**) Displacement data for 1000 h at monitoring point. (**b**) Displacement data recorded by numerical simulation.

Based on the monitoring data, the total displacements at the monitoring point within 1000 h were 0.7008 m in the Y direction, 0.1656 m in the X direction, and −0.6575 m in the Z direction. These correspond to the displacements in the numerical simulation between steps 1600 and 2100. From this, we can infer that the removal at the monitoring point at 1500 h was equivalent to that in the numerical simulation between steps 2400 and 3150. At these moments, the numerical model results showed dy values ranging from 0.884 m to 1.35 m, dx values between 0.42 m and 0.688 m, and dz values from −1.45 m to −2.3 m.

As depicted in Figure 14, the actual monitored displacement results show dy as 1.44 m, dx as 0.20 m, and dz as 1.29 m. There are some differences between the two sets of results, primarily characterized by the overestimation of Z-direction displacement in the numerical simulation and the underestimation of the Y-direction displacement. Additionally, the X-direction displacement in the numerical simulation continued to increase, while the actual monitoring results showed a tendency toward stabilization in the X direction. These differences may be attributed to the fact that, in the natural engineering environment, slope support measures were implemented on both sides of the slope after the excavation of the drainage ditch, limiting the X-direction displacement. The numerical simulation, which did not accurately model this actual situation, resulted in these disparities.

While the numerical simulation did not precisely predict the actual displacements for this specific monitoring point, this three-dimensional numerical modeling still holds significant value in forecasting surface deformations and providing construction references.

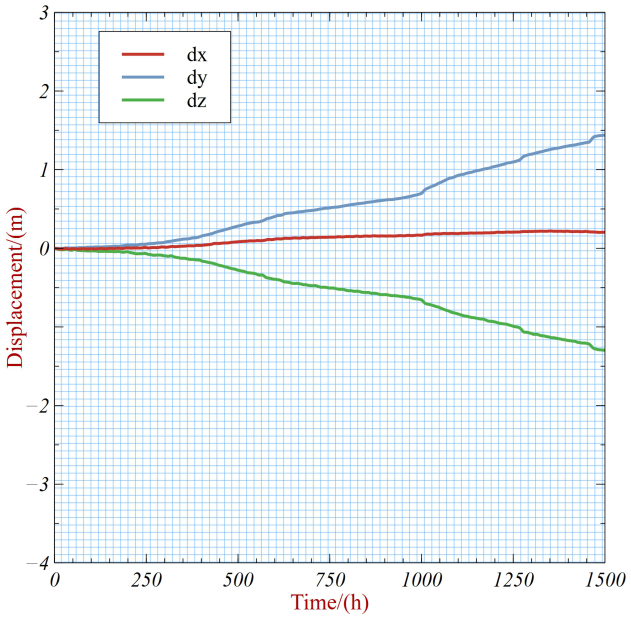

Figure 14. Displacement data for 1500 h at monitoring point.

4. Discussion

Based on the 3D numerical simulation results, new underground mining activities were shown to induce changes on the surface, including intensified subsidence in the mining area and the formation of fractures within the rock and soil. Observing the displacement cloud maps at different simulation stages, it is noteworthy that displacement occurred earliest and most prominently in the areas near the existing subsidence zone. This can be attributed to underground voids from prior mining phases at the base of the subsidence zone, coupled with the dynamic nature of the subsidence itself, resulting in early and significant displacements in this region. Subsequently, the displacement spread to the surrounding areas. However, the simulation results weakened the impact of new mining activities on the existing subsidence due to constraints on the velocities of the overlying rock mass above the subsidence zone. This is inconsistent with actual observations. When the displacement extended to the no-thickness boundary interface set at the south side

of the model, the relatively weak structural strength of the interface led to increasing multi-directional displacement differences in the rock and soil on either side of the interface, resulting in the expansion and widening of fractures.

As shown in Figures 9a and 11b, it is worth noting that the numerical simulation results indicate a certain displacement in the X direction of the rock and soil mass. In the early stages of engineering activities, support measures were implemented for the rocky slopes on both sides after excavating drainage ditches. These measures were believed to be effective in stabilizing the structure. However, new mining activities redistributed stress within the rock and soil mass, potentially affecting the existing support structures. In the actual engineering environment, as shown in Figure 15, it has been observed that some anchor structures have already failed, which is a matter of significant concern.

Figure 15. Pictures of slope anchor failure on the west side of the drainage ditch.

By comparing the numerical simulation results with actual monitoring data, we found that the simulation achieved some success. Despite some differences from the existing monitoring data, predicting the displacement of monitoring points based on the simulation results still holds valuable reference value. As part of an academic article, this passage appropriately addresses the relationship between numerical simulation results, real-world scenarios, and potential engineering implications. It effectively communicates your research findings and their practical applications. In its initial state, the model simulated the rock mass excavation in the southern mining area and analyzed the process of mining-induced collapse. It investigated the slope's crack formation and development patterns under new mining conditions. It conducted a comparative analysis of the impact of mining on the existing subsidence crater.

5. Conclusions

In this study, we investigated the effects of new mining activities on the surface and the formation mechanisms of large-scale fractures on the southern side of the Prang Copper Mine's subsidence area. The following conclusions were drawn:

1. The initiation of new mining activities in the southern part of the Prang Copper Mine's first mining area resulted in ongoing subsidence of the upper surface. Due to the complex interactions between surface and subsurface structures, the surface displacements exhibit non-uniform patterns. The numerical simulation results indicate that, during this process, surface rock layers near the subsidence area experience initial displacements with the highest magnitudes. This phenomenon is closely related to the subsidence of the pre-existing collapse zone. As the subsidence continues, it gradually extends southward, eventually reaching the pre-existing structural weaknesses on the slope surface, forming fractures that evolve into more giant fissures. The simulation results after 4000 steps of this numerical model run show that the top gap width reaches 0.6 m with a vertical offset of 1.8 m;

2. As mining-induced subsidence progresses, the internal structural weaknesses within the rock and soil gradually evolve into fractures and subsequently expand into large fissures. In real-world engineering environments, apart from the effects of subsidence, rainfall may expedite the softening of the rock and soil, further facilitating the expansion of these fissures. If appropriate mitigation measures are not implemented, these fissures could potentially lead to slope sliding and toppling, compromising the stability of underground and surface structures;
3. We observed a similar trend between the simulated and actual displacement curves by comparing the numerical simulation results with data from actual monitoring points. Based on the results of the numerical simulation and 1000 h of monitoring results before the site inspection, the displacement of the monitoring point after 1500 h was predicted to be 0.884–1.35 m in the Y direction, 0.42–0.688 m in the X direction, and −1.45–2.3 m in the Z direction, while the actual monitoring of the site for 1500 h showed that dy was 1.44 m, dx was 0.20 m, and dz was 1.29 m. This shows that the numerical model has some reference value.

Author Contributions: Conceptualization, Z.L. and K.H.; methodology, G.L. and J.T.; software, T.L.; validation, T.L.; formal analysis, J.T.; investigation, T.L.; resources, Z.L.; data curation, T.L. and G.L.; writing—original draft preparation, Z.L.; writing—review and editing, Z.L. and K.H.; visualization, T.L.; supervision, G.L.; project administration, J.T.; funding acquisition, G.L. All authors have read and agreed to the published version of the manuscript.

Funding: This work was supported by the National Natural Science Foundation of China (No. 41974148); the Natural Resources Science and Technology Project of Hunan Province (Grant No. 2022-01); the Transportation Science and Technology Project of Hunan Province (No. 202217); the Science and Technology Research and Development Project of China Railway Co., Ltd. (No. 2022-Special-07-02).

Institutional Review Board Statement: Not applicable.

Informed Consent Statement: Not applicable.

Data Availability Statement: The data used to support the findings of the research are included in this article.

Conflicts of Interest: Author Zhengrong Li was employed by the company Yunnan Diqin Nonferrous Metal Co., Ltd. The remaining authors declare that the research was conducted in the absence of any commercial or financial relationships that could be construed as a potential conflict of interest. The authors declare that this study received funding from the Science and Technology Research and Development Project of China Railway Co., Ltd. The funder was not involved in the study design, collection, analysis, interpretation of data, the writing of this article or the decision to submit it for publication.

References

1. Bazaluk, O.; Petlovanyi, M.; Lozynskyi, V.; Zubko, S.; Sai, K.; Saik, P. Sustainable Underground Iron Ore Mining in Ukraine with Backfilling Worked-Out Area. *Sustainability* **2021**, *13*, 834. [CrossRef]
2. Lapshyn, O.; Khudyk, M. The tragicconsequences of the collapse of the earth's surface within the mining allotment of Ordzhonikidze mine. *E3s Web Conf.* **2020**, *166*, 03003. [CrossRef]
3. Xia, K.; Chen, C.; Liu, X.; Zheng, X.; Zhou, Y.; Song, X.; Yuan, J. Ground collapse and caving mechanisms in strata overlying sublevel caving mines: A case study. *Bull. Eng. Geol. Environ.* **2024**, *83*, 21. [CrossRef]
4. Bruneau, G.; Hudyma, M.; Hadjigeorgiou, J.; Potvin, Y. Influence of faulting on a mine shaft-a case study: Part II-numerical modelling. *Int. J. Rock Mech. Min. Sci.* **2003**, *40*, 113–125. [CrossRef]
5. Hoek, E. Progressive caving induced by mining an inclined orebody. *Trans. Inst. Min. Metall.* **1974**, *83*, A133–A139.
6. Ren, W.; Guo, C.; Peng, Z.; Wang, Y. Model experimental research on deformation and subsidence characteristics of ground and wall rock due to mining under thick overlying terrane. *Int. J. Rock Mech. Min. Sci.* **2010**, *47*, 614–624. [CrossRef]
7. Dai, H.; Lian, X.; Liu, J.; Liu, Y.; Zhou, Y.; Deng, W.; Cai, Y. Model study of deformation induced by fully mechanized caving below a thick loess layer. *Int. J. Rock Mech. Min. Sci.* **2010**, *47*, 1027–1033. [CrossRef]
8. Xia, K.; Chen, C.; Deng, Y.; Xiao, G.; Zheng, Y.; Liu, X.; Fu, H.; Song, X.; Chen, L. In situ monitoring and analysis of the mining-induced deep ground movement in a metal mine. *Int. J. Rock Mech. Min. Sci.* **2018**, *109*, 32–51. [CrossRef]

9. Zhao, H.; Ma, F.; Zhang, Y.; Guo, J. Monitoring and mechanisms of ground deformation and ground fissures induced by cut-and-fill mining in the Jinchuan Mine 2, China. *Environ. Earth Sci.* **2013**, *68*, 1903–1911. [CrossRef]
10. Vyazmensky, A.; Stead, D.; Elmo, D.; Moss, A. Numerical analysis of block caving-induced instability in large open pit slopes: A finite element/discrete element approach. *Rock Mech. Rock Eng.* **2010**, *43*, 21–39. [CrossRef]
11. Salmi, E.F.; Nazem, M.; Karakus, M. Numerical analysis of a large landslide induced by coal mining subsidence. *Eng. Geol.* **2017**, *217*, 141–152. [CrossRef]
12. Laubscher, D. Block caving manual. In *Report for the International Caving Study*; JKMRC and Itasca Consulting Group: Brisbane, Australia, 2000.
13. Woo, K.S.; Eberhardt, E.; Elmo, D.; Stead, D. Empirical investigation and characterization of surface subsidence related to block cave mining. *Int. J. Rock Mech. Min. Sci.* **2013**, *61*, 31–42. [CrossRef]
14. Villegas, T.; Nordlund, E. Numerical analysis of the hangingwall failure at the Kiirunavaara mine. In Proceedings of the International Conference & Exhibition on Mass Mining, Luleå, Sweden, 9–11 June 2008; pp. 867–876. [CrossRef]
15. Shi, Y.; Zhao, M.; Hao, J. Study on numerical models in predicting surface deformation caused by underground coal mining. *Geotech. Geol. Eng.* **2021**, *39*, 4457–4473. [CrossRef]
16. Xu, N.; Kulatilake, P.H.S.W.; Tian, H. Surface subsidence prediction for the WUTONG mine using a 3-D finite difference method. *Comput. Geotech.* **2013**, *48*, 134–145. [CrossRef]
17. Parmar, H.; Yarahmadi, B.A.; Najafi, M. Impact of ground surface subsidence due to underground mining on surface infrastructure: The case of the Anomaly No. 12 Sechahun, Iran. *Environ. Earth Sci.* **2019**, *78*, 409. [CrossRef]
18. Zhao, X.; Yu, W.; Zhao, Y.; Fu, S. Numerical Estimation of Shaft Stability and Surface Deformation Induced by Underground Mining Transferred from Open-Pit Mining in Jinfeng Gold Mine. *Minerals* **2023**, *13*, 196. [CrossRef]
19. Cheng, Q.; Shi, Y.; Zuo, L. Numerical simulation and analysis of surface and surrounding rock failure in deep high-dip coal seam mining. *Geotech. Geol. Eng.* **2019**, *37*, 4285–4299. [CrossRef]
20. Wang, G.; Li, P.; Wu, Q.; Cui, X.; Tan, Z. Numerical simulation of mining-induced damage in adjacent tunnels based on FLAC3D. *Adv. Civ. Eng.* **2021**, *2021*, 9855067. [CrossRef]
21. Huang, G.; Kulatilake, P.H.; Shreedharan, S.; Cai, S.; Song, H. 3D discontinuum numerical modeling of subsidence incorporating ore extraction and backfilling operations in an underground iron mine in China. *Int. J. Min. Sci. Technol.* **2017**, *27*, 191–201. [CrossRef]
22. Xie, J. Stability Study of the Bottom Structure in Progressive Caving Induced by Mining an Inclined Ore Body. Master Thesis, Kunming University of Science and Technology, Kunming, China, 2017.
23. Xie, W.B.; Chen, X.X.; Zheng, B.S. *Research and Analysis on Numerical Simulation Subjects in Mining Engineering*; China University of Mining and Technology Press: Xuzhou, China, 2005. (In Chinese)
24. Kumar, R.; Choudhury, D.; Bhargava, K. Simulation of rock subjected to underground blast using FLAC3D. *Jpn. Geotech. Soc. Spec. Publ.* **2016**, *2*, 508–511. [CrossRef]
25. Vyazmensky, A. Numerical Modelling of Surface Subsidence Associated with Block Cave Mining Using a Finite Element/Discrete Element Approach. Ph.D. Thesis, Fraser University, Burnaby, BC, Canada, 2008.
26. Villegas Barba, T.F.; Nordlund, E. Numerical analyses of the hangingwall failure due to sublevel caving: Study case. *Int. J. Min. Miner. Eng.* **2013**, *4*, 201–223. [CrossRef]
27. Helm, P.R.; Davie, C.T.; Glendinning, S. Numerical modeling of shallow abandoned mine working subsidence affecting transport infrastructure. *Eng. Geol.* **2013**, *154*, 6–19. . [CrossRef]
28. Hoek, E.; Marinos, P. A brief history of the development of the Hoek-Brown failure criterion. *Soils Rocks* **2007**, *30*, 85–92. [CrossRef]

Disclaimer/Publisher's Note: The statements, opinions and data contained in all publications are solely those of the individual author(s) and contributor(s) and not of MDPI and/or the editor(s). MDPI and/or the editor(s) disclaim responsibility for any injury to people or property resulting from any ideas, methods, instructions or products referred to in the content.